



# CHORUS

This is the accepted manuscript made available via CHORUS. The article has been published as:

## Matching lattice and continuum four-fermion operators with nonrelativistic QCD and highly improved staggered quarks

Christopher Monahan, Elvira Gámiz, Ron Horgan, and Junko Shigemitsu (HPQCD Collaboration)

Phys. Rev. D **90**, 054015 — Published 16 September 2014

DOI: [10.1103/PhysRevD.90.054015](https://doi.org/10.1103/PhysRevD.90.054015)

# Matching lattice and continuum four-fermion operators with NRQCD and HISQ quarks

Christopher Monahan

*Physics Department, College of William and Mary, Williamsburg, Virginia 23187, USA*

Elvira Gámiz

*CAFPE and Departamento de Física Teórica y del Cosmos, Universidad de Granada, Granada, España*

Ron Horgan

*DAMTP, Centre for Mathematical Sciences, University of Cambridge, Cambridge, CB3 0WA, UK*

Junko Shigemitsu

*Physics Department, The Ohio State University, Columbus, Ohio 43210, USA*

(HPQCD Collaboration)

We match continuum and lattice heavy-light four-fermion operators at one loop in perturbation theory. For the heavy quarks we use nonrelativistic QCD (NRQCD) and for the massless light quarks the Highly Improved Staggered Quark (HISQ) action. We include the full set of  $\Delta B = 2$  operators relevant to neutral  $B$  mixing both within and beyond the Standard Model and match through order  $\alpha_s$ ,  $\Lambda_{\text{QCD}}/M_b$ , and  $\alpha_s/(aM_b)$ .

PACS numbers: 12.38.Bx,12.38.Gc,13.20.He,14.40.Nd

## I. INTRODUCTION

Despite intense experimental and theoretical effort, there have been no observations of Beyond the Standard Model (BSM) particles. Direct detection at high energy collider experiments is not, however, the only way to uncover evidence for new physics. Indirect detection through high-precision measurements at relatively low energies is also possible. At low energies, new physics appears through quantum loop effects, which can probe energy scales far greater than those available at current high energy experiments, such as at the Large Hadron Collider. Detecting such loop effects requires precise theoretical predictions of Standard Model physics with which to compare experimental data. A related approach is to study the unitarity of the Cabibbo-Kobayashi-Maskawa (CKM) quark mixing matrix. In the Standard Model, the CKM matrix is unitary and deviations from unitarity could indicate the presence of new physics. Multiple, independent determinations over-constrain the CKM parameters, usually expressed in terms of “unitarity triangles”.

Heavy quark flavor physics is one area that could be particularly sensitive to the effects of heavy BSM particles. In particular, neutral  $B$  meson mixing, which is both loop- and CKM-suppressed, provides a promising avenue for new physics searches. In the last decade there have been extensive experimental studies of neutral  $B$  meson mixing and  $B$  decays from the CDF [1, 2], D0 [3–5], and most recently, LHCb [6, 7] Collaborations. Some of these results have exposed a 2-3 $\sigma$  discrepancy between certain Standard Model predictions and measurements [3, 5, 8]. In addition, recent CKM unitarity triangle fits hint at the presence of BSM physics, with some fits fa-

voring new physics contributions in the neutral  $B$  mixing sector [9–12].

Neutral  $B$  meson mixing is characterized by the mass and decay width differences between the “heavy” and “light” mass eigenstates, which are admixtures of quark flavor eigenstates. The mass difference,  $\Delta M_q = M_H - M_L$ , is equivalent to the oscillation frequency of a neutral  $B_q$  meson with light quark species  $q$ . Theoretical studies of neutral  $B$  meson mixing employ effective Hamiltonians that incorporate four-fermion operators. Matrix elements of these operators characterize the nonperturbative Quantum Chromodynamics (QCD) behavior of the mixing process and these matrix elements must be determined with a precision sufficient to confront experimental data with stringent tests. Precise *ab initio* calculations of nonperturbative QCD effects require lattice QCD.

The scope of neutral  $B$  meson mixing calculations on the lattice has been quite extensive and several lattice collaborations have produced results with up/down and strange quarks in the sea [13–17]. The HPQCD Collaboration is currently carrying out nonperturbative calculations that incorporate the effects of up/down, strange, and charm quarks in the sea for the first time [18].

The gauge ensembles that are currently available have a lattice spacing too large to accommodate heavy quarks directly at the physical  $b$  quark mass. Lattice calculations are therefore generally carried out using an effective theory for the heavy quark fields, such as heavy quark effective theory (HQET) or non-relativistic QCD (NRQCD). Effective theories on the lattice must be related to continuum QCD to extract physically meaningful results. In this work we determine the one loop matching coefficients required to relate lattice matrix elements of  $\Delta B = 2$  operators, constructed using the highly improved stag-

gered quark (HISQ) and NRQCD actions, to the corresponding matrix elements in continuum QCD. We match through  $\mathcal{O}(\alpha_s, \Lambda_{QCD}/M_b, \alpha_s/(aM_b))$  and include “subtracted” dimension-seven operators, which remove power law divergences at  $\mathcal{O}(\alpha_s/(aM))$ , only at tree-level.

Our calculation extends the work of [19] to include massless HISQ light quarks and is a significant step in the HPQCD Collaboration’s program to determine improvement and matching coefficients for lattice NRQCD at one loop [20–22]. These matching calculations are an integral component of the HPQCD Collaboration’s precision  $B$  physics effort. Here we largely follow the notation of [19] for consistency and to enable easy comparison with that work. A similar matching calculation for a restricted range of  $\Delta B = 2$  operators in NRQCD was carried out in [23]. Matching calculations for static heavy quarks with a range of light quark actions were undertaken in [24] and more recently in [25–27]. A preliminary discussion of  $\mathcal{O}(1/M_b)$  operators in HQET was presented in [28]. We provide full details of the extraction of the lattice NRQCD mixing coefficients, which does not appear in the literature.

In the next section we discuss four-fermion operators in continuum QCD and on the lattice. We then describe the matching procedure that relates the matrix elements of these operators. In Section IV we detail the calculation of the lattice mixing coefficients. We present our results for the mixing parameters from heavy-light four-fermion operators through order  $\alpha_s$ ,  $\Lambda_{QCD}/M_b$ , and  $\alpha_s/(aM_b)$  in Section V. We conclude with a summary in Section VI. In Appendix A we provide some details of the continuum calculations entering the matching procedure. We discuss two different NDR- $\overline{MS}$  schemes that have been used in the literature for the renormalization of the Standard Model  $\Delta B = 2$  operators  $Q2$  and  $Q3$ , and we correct two errors in Equations (B9) and (B10) of reference [19].

## II. FOUR-FERMION OPERATORS

### A. In continuum QCD

There are three dimension-six,  $\Delta B = 2$  operators that are relevant to neutral  $B$  meson mixing in the Standard Model:

$$Q1 = \left( \overline{\Psi}_b^i \gamma^\mu P_L \Psi_q^i \right) \left( \overline{\Psi}_b^j \gamma_\mu P_L \Psi_q^j \right), \quad (1)$$

$$Q2 = \left( \overline{\Psi}_b^i P_L \Psi_q^i \right) \left( \overline{\Psi}_b^j P_L \Psi_q^j \right), \quad (2)$$

$$Q3 = \left( \overline{\Psi}_b^i P_L \Psi_q^j \right) \left( \overline{\Psi}_b^j P_L \Psi_q^i \right). \quad (3)$$

Here the subscript on the QCD fields,  $\Psi$  and  $\overline{\Psi}$ , denote the quark species:  $b$  for bottom quarks and  $q$  for down or strange quarks, which we take to be massless. The superscripts  $i$  and  $j$  are color indices and  $P_{R,L} = (1 \pm \gamma_5)$  are right- and left-handed projectors. Operator  $Q1$  determines the mass difference  $\Delta M_q$  in the Standard Model

and all three are useful in studies of the width difference  $\Delta\Gamma_q$ .

BSM physics can be parameterized by a  $\Delta B = 2$  effective Hamiltonian, which incorporates two further independent operators,

$$Q4 = \left( \overline{\Psi}_b^i P_L \Psi_q^i \right) \left( \overline{\Psi}_b^j P_R \Psi_q^j \right), \quad (4)$$

$$Q5 = \left( \overline{\Psi}_b^i P_L \Psi_q^j \right) \left( \overline{\Psi}_b^j P_R \Psi_q^i \right). \quad (5)$$

Collectively these five operators are known as the “SUSY basis of operators” in the literature [29]. We simplify intermediate stages of the matching calculation by introducing two extra operators,

$$Q6 = \left( \overline{\Psi}_b^i \gamma_\mu P_L \Psi_q^i \right) \left( \overline{\Psi}_b^j \gamma^\mu P_R \Psi_q^j \right), \quad (6)$$

$$Q7 = \left( \overline{\Psi}_b^i \gamma_\mu P_L \Psi_q^j \right) \left( \overline{\Psi}_b^j \gamma^\mu P_R \Psi_q^i \right). \quad (7)$$

Matrix elements of these operators are related to matrix elements of  $Q5$  and  $Q4$  via Fierz relations, so that, as one would expect,  $Q6$  and  $Q7$  are not independent operators.

Matching calculations in perturbation theory are generally carried out by considering scattering between external quark (or gluon) states. For the case of  $\Delta B = 2$  operators, we consider scattering from an incoming state consisting of a heavy anti-quark and a light quark to an outgoing state of a heavy quark and light anti-quark. We write these states symbolically by

$$|\text{in}\rangle = |\overline{Q}^B; q^C\rangle, \quad \text{and} \quad \langle \text{out} | = \langle \overline{q}^A; Q^D |, \quad (8)$$

where the superscripts are color indices. The corresponding external Dirac spinors are  $u_q$  and  $v_q$  for the incoming light quark and outgoing light anti-quark and  $\overline{u}_Q$  and  $\overline{v}_Q$  for the outgoing heavy quark and incoming heavy anti-quark respectively.

We denote the matrix elements of the operators  $Qi$  by

$$\langle Qi \rangle = \langle \text{out} | Qi | \text{in} \rangle, \quad (9)$$

and at tree-level  $Q1$ ,  $Q2$ ,  $Q4$ , and  $Q6$  are

$$\begin{aligned} & \langle \overline{q}^A; Q^D | \left( \overline{\Psi}_b^i \Gamma_1 \Psi_q^i \right) \left( \overline{\Psi}_b^j \Gamma_2 \Psi_q^j \right) | \overline{Q}^B; q^C \rangle_{\text{tree}} \\ &= \delta_{AB} \delta_{CD} [(\overline{u}_Q \Gamma_1 u_q)(\overline{v}_Q \Gamma_2 v_q) + (\overline{u}_Q \Gamma_2 u_q)(\overline{v}_Q \Gamma_1 v_q)] \\ & \quad - \delta_{AD} \delta_{BC} [(\overline{u}_Q \Gamma_1 v_q)(\overline{v}_Q \Gamma_2 u_q) + (\overline{u}_Q \Gamma_2 v_q)(\overline{v}_Q \Gamma_1 u_q)], \end{aligned} \quad (10)$$

which we represent diagrammatically in Figure 1. The Dirac operators  $\Gamma_{1,2}$  represent the operator insertions corresponding to Equations (1) to (7). For matrix elements of  $Q3$ ,  $Q5$ , and  $Q7$ , we have instead

$$\begin{aligned} & \langle \overline{q}^A; Q^D | \left( \overline{\Psi}_b^i \Gamma_1 \Psi_q^j \right) \left( \overline{\Psi}_b^j \Gamma_2 \Psi_q^i \right) | \overline{Q}^B; q^C \rangle_{\text{tree}} \\ &= \delta_{AD} \delta_{CB} [(\overline{u}_Q \Gamma_1 u_q)(\overline{v}_Q \Gamma_2 v_q) + (\overline{u}_Q \Gamma_2 u_q)(\overline{v}_Q \Gamma_1 v_q)] \\ & \quad - \delta_{AB} \delta_{CD} [(\overline{u}_Q \Gamma_1 v_q)(\overline{v}_Q \Gamma_2 u_q) + (\overline{u}_Q \Gamma_2 v_q)(\overline{v}_Q \Gamma_1 u_q)]. \end{aligned} \quad (11)$$

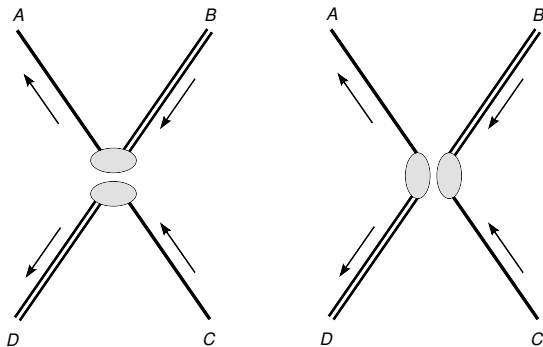


FIG. 1. Tree-level diagrams representing the matrix elements of operators  $Q1$ ,  $Q2$ ,  $Q4$ , and  $Q6$ . The incoming state is a heavy anti-quark and a light quark and the outgoing state is a heavy quark and a light anti-quark. The letters  $A$ ,  $B$ ,  $C$ , and  $D$  are color indices and correspond to the conventions of Equation (10).

Radiative corrections induce mixing between the four-fermion operators, which we write as

$$\langle Q_i \rangle^{\overline{MS}} = \langle Q_i \rangle_{\text{tree}} + \alpha_s c_{ij} \langle Q_j \rangle_{\text{tree}}^{(0)}, \quad (12)$$

where the superscript (0) denotes matrix elements constructed using spinors that obey

$$\bar{u}_Q \gamma_0 = \bar{u}_Q, \quad \text{and} \quad \bar{v}_Q \gamma_0 = -\bar{v}_Q, \quad (13)$$

in order to match to the effective theory. In principle the product  $c_{ij} \langle Q_j \rangle_{\text{tree}}^{(0)}$  is a sum over all operators  $Q_j$  that mix with  $Q_i$ . In practice, however, only two such operators appears: for example, for  $Q1$  we have

$$\langle Q1 \rangle^{\overline{MS}} = \langle Q1 \rangle_{\text{tree}} + \alpha_s c_{11} \langle Q1 \rangle_{\text{tree}}^{(0)} + \alpha_s c_{12} \langle Q2 \rangle_{\text{tree}}^{(0)}. \quad (14)$$

In the following, we leave this sum implicit.

## B. On the lattice

In the effective theory formalism of NRQCD, the heavy quarks and anti-quarks are treated as distinct quark species. We separate the quark fields that create heavy quarks, which we denote  $\underline{\Psi}_Q$ , from the fields that annihilate heavy anti-quarks, which we represent by  $\overline{\Psi}_Q$ .

The two-component heavy quark field is obtained from the four-component QCD quark field,  $\overline{\Psi}_b$ , via the Foldy-Wouthuysen-Tani transformation (see, for example, [30]),

$$\overline{\Psi}_b = \overline{\Psi}_Q \left( 1 + \frac{1}{2M} \gamma \cdot \overleftarrow{\nabla} + \mathcal{O}(1/M^2) \right), \quad (15)$$

where the arrow indicates that the derivative acts on the heavy quark field to the left. We insert this expansion into the four-fermion operators of Equations (1) to (7) to determine the appropriate NRQCD operators. We

see immediately that, at leading order in  $1/M$ , we need operators of the form

$$\widehat{Q}i = (\overline{\Psi}_Q \Gamma_1 \Psi_q) (\overline{\Psi}_Q \Gamma_2 \Psi_q) + (\overline{\Psi}_Q \Gamma_1 \Psi_q) (\overline{\Psi}_Q \Gamma_2 \Psi_q). \quad (16)$$

We obtain the  $\mathcal{O}(\Lambda_{\text{QCD}}/M)$  corrections by introducing the operators

$$\begin{aligned} \widehat{Q}i1 = \frac{1}{2M} & \left[ (\overrightarrow{\nabla} \overline{\Psi}_Q \cdot \gamma \Gamma_1 \Psi_q) (\overline{\Psi}_Q \Gamma_2 \Psi_q) \right. \\ & + (\overline{\Psi}_Q \Gamma_1 \Psi_q) (\overrightarrow{\nabla} \overline{\Psi}_Q \cdot \gamma \Gamma_2 \Psi_q) \\ & + (\overrightarrow{\nabla} \overline{\Psi}_Q \cdot \gamma \Gamma_1 \Psi_q) (\overline{\Psi}_Q \Gamma_2 \Psi_q) \\ & \left. + (\overline{\Psi}_Q \Gamma_1 \Psi_q) (\overrightarrow{\nabla} \overline{\Psi}_Q \cdot \gamma \Gamma_2 \Psi_q) \right]. \quad (17) \end{aligned}$$

We denote the matrix elements of the effective theory by

$$\langle \widehat{Q}i \rangle = \langle \text{out} | \widehat{Q}i | \text{in} \rangle, \quad \text{and} \quad \langle \widehat{Q}i1 \rangle = \langle \text{out} | \widehat{Q}i1 | \text{in} \rangle, \quad (18)$$

where now the “in” and “out” states are understood to be an incoming NRQCD anti-quark and HISQ quark and an outgoing NRQCD quark and HISQ anti-quark, respectively. Radiative corrections induce mixing between these operators, with mixing coefficients  $c_{ij}^{\text{latt}}$ , and we obtain

$$\langle \widehat{Q}i \rangle = \langle \widehat{Q}i \rangle_{\text{tree}}^{(0)} + \alpha_s c_{ij}^{\text{latt}} \langle \widehat{Q}j \rangle_{\text{tree}}^{(0)}, \quad (19)$$

and similarly

$$\langle \widehat{Q}i1 \rangle = \langle \widehat{Q}i1 \rangle_{\text{tree}}^{(0)} + \alpha_s c_{ij}^{\text{latt}} \langle \widehat{Q}j \rangle_{\text{tree}}^{(0)}. \quad (20)$$

We ignore the one loop corrections to  $\langle \widehat{Q}i1 \rangle_{\text{tree}}^{(0)}$ , which only arise at  $\mathcal{O}(\alpha_s \Lambda_{\text{QCD}}/M_b)$  in the matching procedure.

As discussed in more detail in [19], the mixing coefficients  $c_{ij}^{\text{latt}}$  describe the “mixing down” of dimension seven operators  $\widehat{Q}i1$  onto dimension six operators  $\widehat{Q}j$ .

In the next section we outline the matching procedure before describing the calculation of the lattice mixing coefficients.

## III. THE MATCHING PROCEDURE

We now relate the matrix elements of the NRQCD-HISQ operators, which ultimately will be determined nonperturbatively on the lattice, to the matrix elements of QCD operators in the  $\overline{MS}$  scheme. In other words, we wish to relate Equations (19) and (20) to Equation (12).

We first expand the QCD matrix element  $\langle Q_i \rangle_{\text{tree}}$  in Equation (12) in powers of the inverse heavy quark mass:

$$\langle Q_i \rangle_{\text{tree}} = \langle Q_i \rangle_{\text{tree}}^{(0)} + \langle Q_i1 \rangle_{\text{tree}}^{(0)}. \quad (21)$$

Thus the QCD matrix element becomes

$$\langle Q_i \rangle^{\overline{MS}} = \langle Q_i \rangle_{\text{tree}}^{(0)} + \langle Q_i1 \rangle_{\text{tree}}^{(0)} + \alpha_s c_{ij} \langle Q_j \rangle_{\text{tree}}^{(0)}. \quad (22)$$

Our aim is to write the QCD matrix element in terms of the NRQCD-HISQ matrix elements. Therefore we need to re-express the tree-level matrix elements  $\langle Qi \rangle_{\text{tree}}^{(0)}$  and  $\langle Qi1 \rangle_{\text{tree}}^{(0)}$  in terms of the matrix elements on the lattice. To achieve this, we invert Equations (19) and (20) to obtain

$$\langle \widehat{Q}i \rangle_{\text{tree}}^{(0)} = \langle \widehat{Q}i \rangle - \alpha_s c_{ij}^{\text{latt}} \langle \widehat{Q}j \rangle, \quad (23)$$

and

$$\langle \widehat{Q}i1 \rangle_{\text{tree}}^{(0)} = \langle \widehat{Q}i1 \rangle - \alpha_s \zeta_{ij}^{\text{latt}} \langle \widehat{Q}j \rangle. \quad (24)$$

Using

$$\langle \widehat{Q}i \rangle_{\text{tree}}^{(0)} = \langle Qi \rangle_{\text{tree}}^{(0)}, \quad \text{and} \quad \langle \widehat{Q}i1 \rangle_{\text{tree}}^{(0)} = \langle Qi1 \rangle_{\text{tree}}^{(0)}, \quad (25)$$

we can now plug these results into Equation (22) to find

$$\begin{aligned} \langle Qi \rangle^{\overline{MS}} &= [1 + \alpha_s \rho_{ii}] \langle \widehat{Q}i \rangle + \alpha_s \rho_{ij} \langle \widehat{Q}j \rangle + \langle \widehat{Q}i1 \rangle \\ &\quad - \alpha_s \zeta_{ij}^{\text{latt}} \langle \widehat{Q}j \rangle + \mathcal{O}(\alpha_s^2, \alpha_s \Lambda_{\text{QCD}}/M), \end{aligned} \quad (26)$$

where the matching coefficients,  $\rho_{ij}$ , are given by

$$\rho_{ij} = c_{ij} - c_{ij}^{\text{latt}}. \quad (27)$$

We now define the “subtracted” matrix elements, which remove power law divergences at  $\mathcal{O}(\alpha_s/(aM))$  [19], as

$$\langle \widehat{Q}i1 \rangle_{\text{sub}} = \langle \widehat{Q}i1 \rangle - \alpha_s \zeta_{ij}^{\text{latt}} \langle \widehat{Q}j \rangle, \quad (28)$$

so that our final expression is

$$\begin{aligned} \langle Qi \rangle^{\overline{MS}} &= \langle \widehat{Q}i \rangle + \alpha_s \rho_{ij} \langle \widehat{Q}j \rangle + \langle \widehat{Q}i1 \rangle_{\text{sub}} \\ &\quad + \mathcal{O}(\alpha_s^2, \alpha_s \Lambda_{\text{QCD}}/M). \end{aligned} \quad (29)$$

For a more comprehensive discussion of power law divergences in lattice NRQCD see [31] and [32].

#### IV. EVALUATION OF LATTICE MIXING COEFFICIENTS

Complete details of the lattice actions used in our matching procedure were given in [22] and here we simply summarise the relevant information. For the gauge fields we use the Symanzik improved gauge action with tree level coefficients [33–36], because radiative improvements to the gluon action do not contribute to the matching calculation at one loop [22]. We include a gauge-fixing term and, where possible, we confirm that gauge invariant quantities are gauge parameter independent by working in both Feynman and Landau gauges.

We discretize the light quarks using the HISQ action [37] and set the bare light quark mass to zero. For the heavy quark fields, we use the tree-level NRQCD action of [20, 22]. We do not consider the effects of radiative improvement of the NRQCD action, which are not required for our one loop calculation.

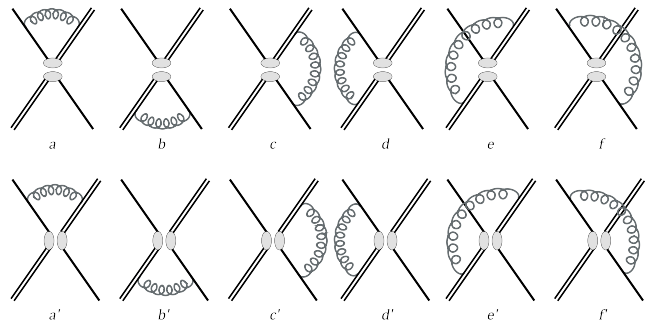


FIG. 2. One loop diagrams representing the corrections to matrix elements of the operators  $Qi$ . The external states are those of Figure 1 and Equation (10).

Our results were obtained using two independent methods: with the automated lattice perturbation theory routines HIPPY and HPSRC [38, 39]; and with **Mathematica** and **FORTRAN** routines developed for earlier matching calculations [22, 40]. We described both of these methods in detail in [22].

We undertook a number of checks of our results. We reproduced the results of [19] with NRQCD heavy quarks and AsqTad light quarks to test the automated lattice perturbation theory routines. In many cases, we established that gauge invariant quantities, such as the mass renormalization, are gauge parameter independent by working in both Feynman and Landau gauges. Furthermore, we carried out several diagram specific checks, which we discuss in more detail in the next subsections.

Finally, we confirmed that infrared divergent parameters, such as the wavefunction renormalization and certain matching parameters, exhibited the correct continuum-like behavior.

As with the heavy-light current matching results of [22], we believe that these two methods are sufficiently independent that agreement between these methods provides a stringent check of our results.

##### A. Dimension six operators

The spinor structures corresponding to the one loop contributions to the matrix elements of the dimension six operators of Equation (19) can be written schematically as the product of two spinor bilinears, each with some particular Lorentz and color structure specified by the precise contribution in question. We illustrate the corresponding Feynman diagrams in Figure 2. This idea schematically generalizes the tree-level results of Equations (10) and (11).

With this schematic in mind, we can break down the diagrams of Figure 2 into two types: those diagrams in which a gluon propagator connects each spinor bilinear and those without such a propagator connection. It is straightforward to recognize that diagrams a), b), c'),

and d') of Figure 2 fall into the latter category and all others into the former. In the following, we focus the discussion on the determination of mixing coefficients for  $\widehat{Q}1$ ,  $\widehat{Q}2$ ,  $\widehat{Q}4$ , and  $\widehat{Q}6$ . We discuss  $\widehat{Q}3$ ,  $\widehat{Q}5$ , and  $\widehat{Q}7$  at the end of this subsection.

### 1. Diagrams a) and b)

Diagrams a) and b) are the most straightforward to compute, since we can separate the spinor bilinears. Diagrams c') and d') are similarly straightforward, but only contribute to  $\widehat{Q}3$ ,  $\widehat{Q}5$ , and  $\widehat{Q}7$ , which we discuss later. The contribution to  $\widehat{Q}1$  from diagram a) is given by

$$a) = \frac{4}{3} \delta_{AB} \delta_{CD} \left( \bar{u}_Q \gamma^\mu P_L u_q \right) \left( \bar{v}_Q \mathcal{V}_\mu v_q \right), \quad (30)$$

where  $\mathcal{V}_\mu$  represents the one loop vertex correction to the heavy-light quark bilinear  $\bar{v}_Q \gamma_\mu P_L v_q$ :

$$\mathcal{V}_\mu = V_{\overline{Q}Qg}^\nu G_{\overline{Q}} \gamma_\mu P_L G_q V_{qqg}^\sigma K_{\nu\sigma}. \quad (31)$$

Here the  $V^\nu$  represent the quark-quark-gluon vertices,  $G_{\overline{Q}}$  the heavy anti-quark propagator and  $G_q$  the quark propagator, and  $K_{\nu\sigma}$  the gluon propagator. Note that, for the other operators in the SUSY basis, there is no occurrence of  $\gamma_\mu$  in the operator insertions and consequently diagram a) takes the form

$$a) = \frac{4}{3} \delta_{AB} \delta_{CD} \left( \bar{u}_Q P_{L,R} u_q \right) \left( \bar{v}_Q \mathcal{V} v_q \right), \quad (32)$$

where

$$\mathcal{V} = V_{\overline{Q}Qg}^\nu G_{\overline{Q}} P_{L,R} G_q V_{qqg}^\sigma K_{\nu\sigma}. \quad (33)$$

We have chosen a specific combination of external colors that isolates the contribution proportional to the spinor bilinears  $\bar{u}_Q \gamma^\mu P_L u_q$  and  $\bar{v}_Q \gamma^\mu P_L v_q$  (compare to Equation (10)), with color factor  $(4/3) \delta_{AB} \delta_{CD}$ . We could equally have chosen to isolate the spinor structure proportional to  $\bar{u}_Q \gamma^\mu P_L v_q$  and  $\bar{v}_Q \gamma^\mu P_L u_q$  with color factor  $(-4/3) \delta_{AD} \delta_{BC}$ . This choice would have given identical results. In the following discussion we leave the color factor implicit for clarity and always work with the contribution to  $\mathcal{O}1$  (analogous relations hold for the other operators).

We separate out the temporal and spatial components so that, for diagram a), for example, we write

$$a) = c_0 \left( \bar{u}_Q \gamma^0 P_L u_q \right) \left( \bar{v}_Q \gamma^0 P_L v_q \right) + \sum_{k=1}^3 c_k \left( \bar{u}_Q \gamma^k P_L u_q \right) \left( \bar{v}_Q \gamma^k P_L v_q \right). \quad (34)$$

By symmetry of the spatial directions, the three coefficients  $c_k$ , for  $k \in \{1, 2, 3\}$ , are all equal. In terms of the

operator mixing of Equation (19), we also have

$$a) = c_{11}^{\text{latt}} \left( \bar{u}_Q \gamma^\mu P_L u_q \right) \left( \bar{v}_Q \gamma_\mu P_L v_q \right) + c_{12}^{\text{latt}} \left( \bar{u}_Q P_L u_q \right) \left( \bar{v}_Q P_L v_q \right). \quad (35)$$

Therefore, by projecting out the coefficient of each spinor structure in Equation (34), we can obtain the mixing coefficients from

$$c_{11}^{\text{latt}} = c_k, \quad \text{and} \quad c_{12}^{\text{latt}} = c_k - c_0. \quad (36)$$

In the automated lattice perturbation theory routines used in this calculation, the result of a generic Feynman diagram integral is expressed as a “spinor”, which is a derived type specified by the HPSRC module `mod_spinors.F90` [38, 39]. The `spinor` type incorporates a 16-element array that specifies the coefficient of each element of the Dirac algebra. Therefore, to extract the coefficient of some particular Dirac structure, all one needs to do is return the corresponding element of the `spinor` array (external spinors are dropped for the purposes of the calculation).

For example, to determine  $c_k$  for diagram a) we extract the coefficient of, say,  $\gamma_3$  from the integrated expression for the Feynman diagram. This corresponds exactly to the standard continuum procedure of multiplying by an appropriate projector and taking the trace, which is the method applied in our second, `Mathematica` / `FORTRAN`, approach to this calculation.

We applied two sets of cross-checks to our results for these diagrams. First, we checked that diagrams a) and b) give identical results. Second, we confirmed that the mixing coefficients were equal to the corresponding heavy-light current results of [22]:

$$c_{11}^{\text{latt}, a) = \zeta_{11}^{(V_k)}, \quad c_{22}^{\text{latt}, a) = \zeta_{11}^{(V_0)}, \quad c_{12}^{\text{latt}, a) = \zeta_{11}^{(V_k)} - \zeta_{11}^{(V_0)}. \quad (37)$$

Note that these  $\zeta_{11}^{(V_\mu)}$  are not the mixing coefficients of the  $1/M$  operators described above (which we denote  $\zeta_{ij}^{\text{latt}}$ ), but the mixing coefficients of the heavy-light currents described in [22].

### 2. Diagrams c) to f')

The calculation of the contributions from diagrams c) to f') of Figure 2 proceed along conceptually similar lines, although the integrand structure is more complicated.

We will examine two examples of the possible spinor structure to illustrate our method. The other diagrams follow the same pattern, *mutatis mutandis*.

The contribution to  $\widehat{Q}1$  from diagram c) is given by

$$c) = -\frac{1}{6} \delta_{AB} \delta_{CD} \left( \bar{u}_Q \mathcal{V}^{(1)\mu\nu} u_q \right) \left( \bar{v}_Q \mathcal{V}_{\mu\nu}^{(2)} v_q \right), \quad (38)$$

where, using the notation described below Equation (31),

$$\mathcal{V}^{(1)\mu\nu} = \gamma^\mu P_L G_q V_{qqg}^\nu, \quad \mathcal{V}_{\mu\nu}^{(2)} = V_{\overline{Q}Qg}^\sigma G_{\overline{Q}} \gamma_\mu P_L K_{\sigma\nu}. \quad (39)$$

Once again we separate out the temporal and spatial contributions to the diagram, akin to Equation (34), and determine the mixing coefficients from

$$c_{11}^{\text{latt}} = c_k, \quad \text{and} \quad c_{12}^{\text{latt}} = c_k - c_0. \quad (40)$$

The procedure for diagram  $a'$ ) is much the same. This time the starting point is (note the different spinor structure)

$$a') = \frac{1}{2} \delta_{AB} \delta_{CD} (\bar{u}_Q \mathcal{V}^{(1)\mu\nu} v_q) (\bar{v}_{\bar{Q}} \mathcal{V}_{\mu\nu}^{(2)} u_q), \quad (41)$$

with  $\mathcal{V}^{(1)\mu\nu}$  and  $\mathcal{V}_{\mu\nu}^{(2)}$  given in Equation (39).

For these diagrams, we confirmed that the contributions from the pairs of diagrams c) and d),  $a'$ ) and  $b'$ ), and  $c'$ ) and  $d'$ ), are each identical.

### 3. Operators $\hat{Q}3$ and $\hat{Q}5$

The previous discussion focussed on the extraction of the mixing coefficients for  $\hat{Q}1$ ,  $\hat{Q}2$ ,  $\hat{Q}4$ , and  $\hat{Q}6$ , which all have the same color structure. The contributions from  $\hat{Q}3$ ,  $\hat{Q}5$  and  $\hat{Q}7$  have a different color structure. It is straightforward to observe, however, that by judicious choice of external colors and appropriate Fierz relations, the contributions to these operators can be related to those from operators  $\hat{Q}2$ ,  $\hat{Q}4$ , and  $\hat{Q}6$ .

For example, one can compare the term proportional to  $\delta_{AB} \delta_{CD}$  for  $\hat{Q}2$  with that proportional to  $\delta_{AD} \delta_{BC}$  for  $\hat{Q}3$  and then, taking into account the relative color factors, one finds

$$\begin{aligned} c_{33}^{\text{latt}, a)/b)} &= \frac{1}{3} c_{33}^{\text{latt}, c')/d')} = -\frac{1}{8} c_{22}^{\text{latt}, a)/b)}, \\ c_{33}^{\text{latt}, c)/d)} &= -8 c_{22}^{\text{latt}, c)/d)}, \\ c_{33}^{\text{latt}, e)} &= c_{22}^{\text{latt}, e)}, \quad c_{33}^{\text{latt}, e')} = c_{22}^{\text{latt}, e')}, \\ c_{33}^{\text{latt}, f)} &= c_{22}^{\text{latt}, f)}, \quad c_{33}^{\text{latt}, f')} = c_{22}^{\text{latt}, f')}. \end{aligned} \quad (42)$$

We have verified by explicit calculation for a specific choice of heavy quark mass that these relations hold.

Combined with the appropriate Fierz identities, these results reduce the number of integrations we must carry out. This significantly speeds up the matching procedure, because there are approximately 80 non-zero coefficient contributions that must be determined at each heavy quark mass for the complete matching calculation.

### B. Dimension seven operators

We represent the diagrams that include the  $1/M$  operators,  $\hat{Q}i1$ , in Figure 3. Note that diagrams in which the derivative acts directly on an external heavy quark or anti-quark vanish, because these external states have zero spatial momentum.

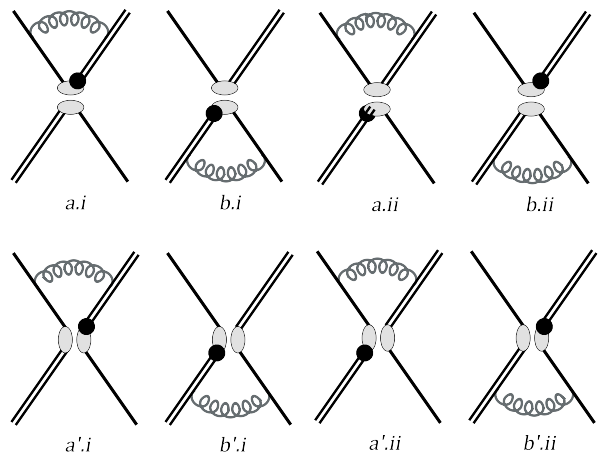


FIG. 3. Sample one loop diagrams representing the corrections to matrix elements of the  $1/M$  operators  $\hat{Q}j1$ . The black dot represents a derivative acting on the heavy (anti-)quark propagator. The external states are those of Figure 1. We show the corrections associated with diagrams a), b),  $a'$ ), and  $b'$ ) of Figure 2. Analogous diagrams exist for diagrams c) to f'). In general diagrams such as  $a.ii$  and  $b.ii$  vanish, because the derivative acts on an external heavy (anti-) quark with zero momentum.

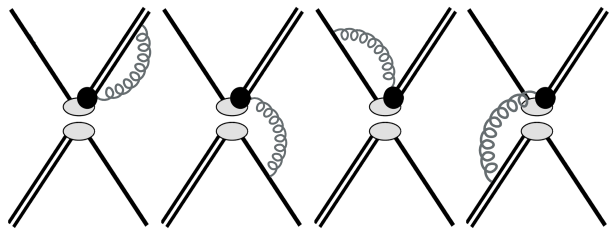


FIG. 4. Sample one loop diagrams representing the one loop corrections to matrix elements of the  $1/M$  operators  $\hat{Q}j1$ . We show the four corrections associated with diagram a) of Figure 2. Analogous diagrams exist for diagrams b) to f'). For more details, see the caption of Figure 2. We do not include these contributions in our matching procedure.

We expect that the systematic truncation uncertainty is dominated by missing terms of  $\mathcal{O}(\alpha_s^2)$  and therefore we do not include contributions that appear at  $\mathcal{O}(\alpha_s \Lambda_{\text{QCD}}/M_b)$ , which we illustrate in Figure 4. These contributions are generated by gluon emission at the  $1/M$  operator vertex and, to our knowledge, have not been calculated in continuum QCD.

The extraction of the mixing coefficients,  $c_{ij}^{\text{latt}}$ , for the  $1/M$  operators parallels that for the leading order operators, with two small differences. The first is the inclusion of a derivative acting on the heavy (anti-)quark propagator. The second is the presence of the extra gamma matrix in the operator, which means that the result is extracted from the coefficient of a different element of the Dirac algebra than in the leading order case. These changes aside, the process is the same.

TABLE I. Infrared finite contributions to the one loop wavefunction renormalization in NRQCD. All results use stability parameter  $n = 4$ . We implement tadpole improvement with the Landau link definition of  $u_0$ . All results are in Feynman gauge. The statistical uncertainties from the numerical integration of the relevant diagrams are unity in the final digit.

$aM_0$	3.297	3.263	3.25	2.66	2.62	1.91	1.89
$C_H$	-0.235	-0.241	-0.244	-0.366	-0.374	-0.617	-0.627

The results are all infrared finite, which we confirm by explicit calculation at different values of the gluon masses. Furthermore we verify that

$$\zeta_{11}^{\text{latt}, a/b) = \zeta_{10}^{(V_k)}, \quad \text{and} \quad \zeta_{12}^{\text{latt}, a/b) = \zeta_{10}^{(V_k)} - \zeta_{10}^{(V_0)}, \quad (43)$$

where the  $\zeta_{10}^{(V_\mu)}$  are the heavy-light current matching results of [22].

### C. Wavefunction renormalization

To complete the matching calculation we also require the HISQ and NRQCD wavefunction renormalization contributions. The one loop parameters of NRQCD have been extensively studied in the literature, for example in [20, 22, 40, 41] and we describe the complete one loop calculations for both massless and massive HISQ in [22]. For the purposes of this work, we need only the massless HISQ result:

$$Z_q = 1 - \alpha_s \left[ C_q + \frac{1}{3\pi} [1 - (1 - \xi)] \log(a^2 \lambda^2) \right] + \mathcal{O}(\alpha_s^2), \quad (44)$$

where  $a\lambda$  is a gluon mass introduced to regulate the infrared divergence. Here  $\xi$  is the gauge-fixing parameter: for Feynman gauge,  $\xi = 1$ . The infrared finite contribution,  $C_q$ , is  $C_q = 0.3940(3)$  in Feynman gauge.

The NRQCD wavefunction renormalization,  $Z_H$ , is given by

$$Z_H = 1 + \alpha_s \left[ C_H - \frac{1}{3\pi} [2 + (1 - \xi)] \log(a^2 \lambda^2) \right] + \mathcal{O}(\alpha_s^2). \quad (45)$$

We tabulate the infrared finite contribution,  $C_H$ , in Table I. We present results with the tree-level NRQCD coefficients,  $c_i = 1$ , and use the Landau link definition of the tadpole improvement factor  $u_0$ , with  $u_0^{(1)} = 0.7503(1)$ . All results use stability parameter  $n = 4$ .

In the following, we incorporate the wavefunction renormalizations,  $Z_q$  and  $Z_Q$ , in the mixing coefficients  $c_{ij}$  with  $i = j$ .

## V. RESULTS

### A. In continuum QCD

The mixing coefficients defined in Equation (12),  $c_{ij}$ , are given to  $\mathcal{O}(\alpha_s)$  in [19]. Coefficients  $c_{11}$ ,  $c_{12}$ ,  $c_{22}$ , and  $c_{21}$  were first published in [23]. Here we collect the results for the mixing coefficients for completeness. We discuss the continuum one loop calculation in more detail in Appendix A, where we focus on the scheme dependence of the “evanescent” operators that enter the matching procedure and correct Equations (B9) and (B10) of [19].

The non-zero coefficients for the Standard Model operators in the “BBGLN” scheme of [42] are

$$c_{11} = \frac{1}{4\pi} \left\{ -\frac{35}{3} - 2 \log \frac{\mu^2}{M^2} - 4 \log \frac{\lambda^2}{M^2} \right\}, \quad (46)$$

$$c_{12} = -\frac{8}{4\pi}, \quad (47)$$

$$c_{22} = \frac{1}{4\pi} \left\{ 10 + \frac{16}{3} \log \frac{\mu^2}{M^2} - \frac{4}{3} \log \frac{\lambda^2}{M^2} \right\}, \quad (48)$$

$$c_{21} = \frac{1}{4\pi} \left\{ \frac{3}{2} + \frac{1}{3} \log \frac{\mu^2}{M^2} + \frac{2}{3} \log \frac{\lambda^2}{M^2} \right\}, \quad (49)$$

$$c_{33} = \frac{1}{4\pi} \left\{ -2 - \frac{8}{3} \log \frac{\mu^2}{M^2} - \frac{4}{3} \log \frac{\lambda^2}{M^2} \right\}, \quad (50)$$

$$c_{31} = \frac{1}{4\pi} \left\{ 3 + \frac{4}{3} \log \frac{\mu^2}{M^2} + \frac{2}{3} \log \frac{\lambda^2}{M^2} \right\}, \quad (51)$$

while the mixing coefficients for the remaining operators in the SUSY basis are

$$c_{44} = \frac{1}{4\pi} \left\{ \frac{143}{12} + 8 \log \frac{\mu^2}{M^2} - \frac{7}{2} \log \frac{\lambda^2}{M^2} \right\}, \quad (52)$$

$$c_{45} = \frac{1}{4\pi} \left\{ -\frac{23}{4} - \frac{3}{2} \log \frac{\lambda^2}{M^2} \right\}, \quad (53)$$

$$c_{55} = \frac{1}{4\pi} \left\{ -\frac{85}{12} - \log \frac{\mu^2}{M^2} - \frac{7}{2} \log \frac{\lambda^2}{M^2} \right\}, \quad (54)$$

$$c_{54} = \frac{1}{4\pi} \left\{ \frac{13}{4} + 3 \log \frac{\mu^2}{M^2} - \frac{3}{2} \log \frac{\lambda^2}{M^2} \right\}. \quad (55)$$

In addition, we require the mixing coefficients for the intermediate operators  $Q6$  and  $Q7$  of Equations (6) and (7), which are given by

$$c_{46} = \frac{1}{4\pi} \left\{ \frac{23}{8} + \frac{3}{4} \log \frac{\lambda^2}{M^2} \right\}. \quad (56)$$

$$c_{57} = \frac{1}{4\pi} \left\{ -\frac{13}{8} - \frac{3}{2} \log \frac{\mu^2}{M^2} + \frac{3}{4} \log \frac{\lambda^2}{M^2} \right\}. \quad (57)$$

### B. On the lattice

We tabulate the infrared finite contributions to the one loop lattice coefficients in Table II. For a breakdown of the individual contributions to the mixing coefficients,

TABLE II. One-loop lattice coefficients,  $c_{ij}^{\text{latt}}$ , for HISQ-NRQCD  $\Delta B = 2$  operators. We include only the infrared finite contributions to the coefficients. The statistical uncertainties from the numerical integration of the relevant diagrams are  $\pm 0.002$ .

$aM_0$	3.297	3.263	3.25	2.66	2.62	1.91	1.89
$c_{11}^{\text{latt}}$	0.208	0.197	0.194	0.008	-0.005	-0.374	-0.389
$c_{12}^{\text{latt}}$	-0.720	-0.727	-0.730	-0.865	-0.877	-1.138	-1.150
$c_{22}^{\text{latt}}$	0.450	0.448	0.447	0.417	0.417	0.337	0.335
$c_{21}^{\text{latt}}$	-0.052	-0.051	-0.051	-0.030	-0.032	0.000	0.001
$c_{33}^{\text{latt}}$	0.090	0.086	0.083	-0.015	-0.021	-0.230	-0.239
$c_{31}^{\text{latt}}$	-0.008	-0.006	-0.004	0.021	0.023	0.072	0.073
$c_{44}^{\text{latt}}$	0.832	0.830	0.829	0.816	0.818	0.792	0.791
$c_{45}^{\text{latt}}$	0.039	0.036	0.036	-0.018	-0.023	-0.124	-0.129
$c_{55}^{\text{latt}}$	0.202	0.195	0.192	0.060	0.052	-0.204	-0.215
$c_{54}^{\text{latt}}$	0.488	0.489	0.490	0.522	0.525	0.587	0.591

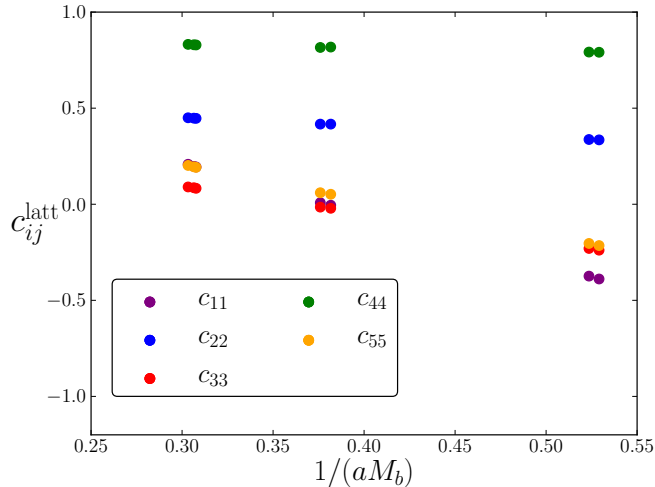


FIG. 5. Mass dependence of the lattice coefficients  $c_{ij}^{\text{latt}}$ , for  $i = j$  [color online]. Statistical uncertainties from numerical integration are  $\pm 0.002$  and smaller than the data points on this scale.

see [19], which demonstrates how one obtains the final result for  $c_{44}^{\text{latt}}$  and  $c_{46}^{\text{latt}}$  and recovers the continuum infrared behavior. For illustration, we plot the mass dependence of the coefficients  $c_{ij}^{\text{latt}}$ , for  $i = j$  and  $i \neq j$ , in Figures 5 and 6, respectively. Note that the scales on the vertical axes of these two plots are identical, to enable easy comparison.

### C. Matching coefficients

Tables III and IV summarise the final results of our calculation. Table III lists the leading-order matching

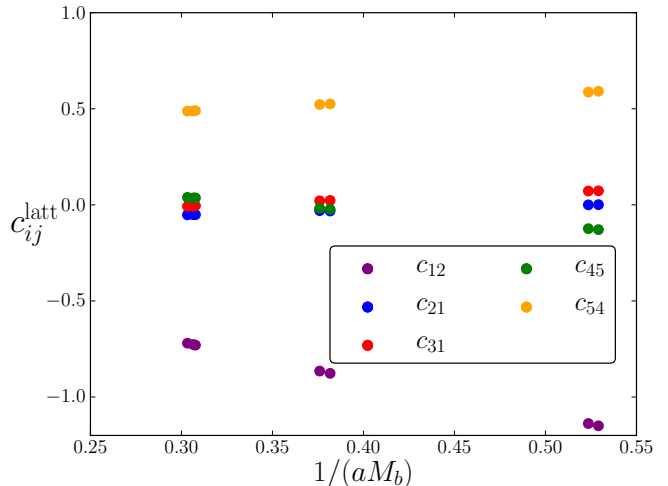


FIG. 6. Mass dependence of the lattice coefficients  $c_{ij}^{\text{latt}}$ , for  $i \neq j$  [color online]. Statistical uncertainties from numerical integration are  $\pm 0.002$  and smaller than the data points on this scale.

TABLE III. One-loop matching coefficients for HISQ-NRQCD  $\Delta B = 2$  operators. The statistical uncertainties from the numerical integration of the relevant diagrams are  $\pm 0.002$ .

$aM_0$	3.297	3.263	3.25	2.66	2.62	1.91	1.89
$\rho_{11}$	-0.377	-0.373	-0.372	-0.314	-0.310	-0.142	-0.134
$\rho_{12}$	0.083	0.090	0.093	0.227	0.238	0.507	0.513
$\rho_{22}$	0.599	0.599	0.599	0.586	0.583	0.596	0.596
$\rho_{21}$	0.045	0.045	0.045	0.059	0.049	0.051	0.051
$\rho_{33}$	0.004	0.006	0.008	0.063	0.066	0.208	0.215
$\rho_{31}$	0.120	0.119	0.119	0.114	0.114	0.098	0.098
$\rho_{44}$	0.781	0.777	0.776	0.677	0.667	0.517	0.512
$\rho_{45}$	-0.212	-0.211	-0.212	-0.206	-0.205	-0.179	-0.177
$\rho_{55}$	-0.101	-0.100	-0.099	-0.079	-0.079	0.001	0.006
$\rho_{54}$	0.055	0.052	0.050	-0.030	-0.036	-0.174	-0.180

coefficients,  $\rho_{ij}$ , at a range of heavy quark masses and at a scale equal to the heavy quark mass. We tabulate next-to-leading contributions,  $\zeta_{ij}$ , in Table IV. We plot the leading order coefficients  $\rho_{ij}$  in Figures 7 and 8, and the next-to-leading order coefficients  $\zeta_{ij}$  in Figures 9 and 10. We use the same vertical axes to simplify comparison between Figures 7 and 8 and between Figures 9 and 10. We choose heavy quark masses that correspond to the HPQCD Collaboration's ongoing nonperturbative calculations of neutral  $B$  mixing [18]. These masses are a subset of those presented in the matching calculation of [22].

TABLE IV. Next-to-leading order matching coefficients for HISQ-NRQCD  $\Delta B = 2$  operators. The statistical uncertainties from the numerical integration of the relevant diagrams are  $\pm 0.002$ .

$aM_0$	3.297	3.263	3.25	2.66	2.62	1.91	1.89
$\zeta_{11}$	0.095	0.096	0.097	0.115	0.117	0.154	0.155
$\zeta_{12}$	0.382	0.386	0.387	0.462	0.467	0.615	0.620
$\zeta_{22}$	0.159	0.161	0.161	0.192	0.165	0.256	0.258
$\zeta_{21}$	0.004	0.004	0.004	0.005	0.005	0.006	0.006
$\zeta_{33}$	-0.032	-0.032	-0.032	-0.038	-0.039	-0.051	-0.052
$\zeta_{31}$	0.028	0.028	0.028	0.034	0.034	0.045	0.045
$\zeta_{44}$	0.135	0.137	0.137	0.163	0.166	0.218	0.220
$\zeta_{45}$	0.040	0.040	0.040	0.048	0.049	0.064	0.065
$\zeta_{55}$	0.040	0.040	0.040	0.048	0.049	0.064	0.065
$\zeta_{54}$	-0.056	-0.056	-0.056	-0.067	-0.068	-0.090	-0.090

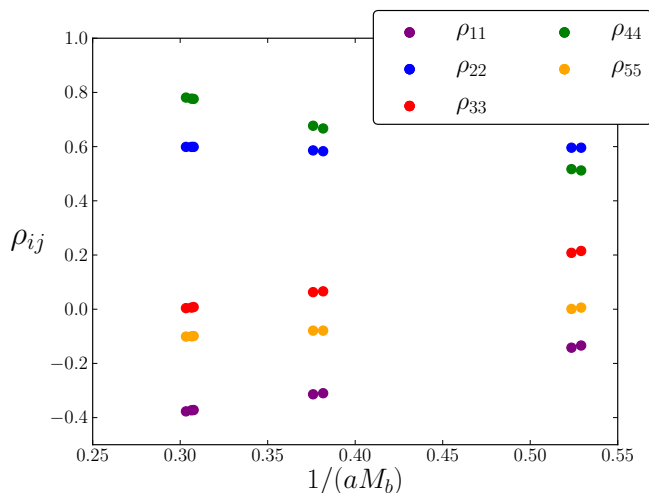


FIG. 7. Mass dependence of the leading order matching coefficients  $\rho_{ij}$ , for  $i = j$  [color online]. Statistical uncertainties from numerical integration are  $\pm 0.002$  and smaller than the data points on this scale.

## VI. SUMMARY

We have determined the one loop matching coefficients required to match the matrix elements of heavy-light four-fermion operators on the lattice to those in continuum QCD. We used NRQCD for the heavy quarks and massless HISQ light quarks. We incorporated the full set of five independent  $\Delta B = 2$  operators relevant to neutral  $B$  mixing both within and beyond the Standard Model and carried out the matching procedure through  $\mathcal{O}(\alpha_s, \Lambda_{\text{QCD}}/M_b, \alpha_s/(aM_b))$ . The perturbative coefficients are well-behaved and all are smaller than unity.

The dominant systematic uncertainties in our matching procedure appear at  $\mathcal{O}(\alpha_s^2)$  with next-to-leading con-

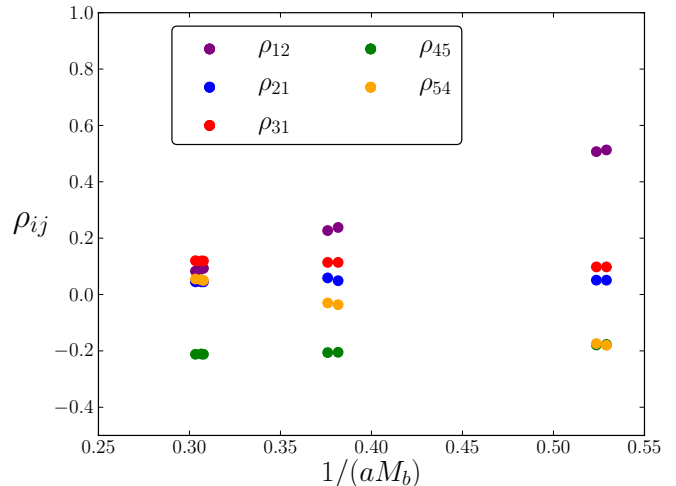


FIG. 8. Mass dependence of the matching coefficients  $\rho_{ij}$ , for  $i \neq j$  [color online].

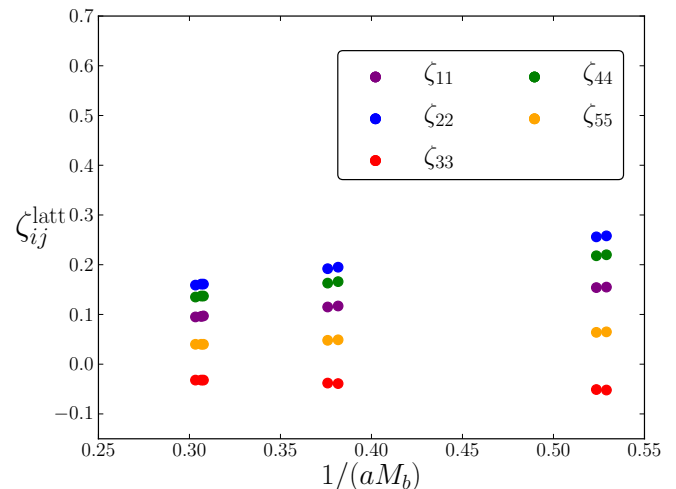


FIG. 9. Mass dependence of the next-to-leading order matching coefficients  $\zeta_{ij}$ , for  $i = j$  [color online]. Statistical uncertainties from numerical integration are  $\pm 0.002$  and smaller than the data points on this scale.

tributions at  $\mathcal{O}(\alpha_s \Lambda_{\text{QCD}}/M_b)$ , the exact values of which will depend on the choice of lattice spacing and matching scale. We estimate that these uncertainties will correspond to a systematic uncertainty of approximately a few percent in the final results for nonperturbative matrix elements in the  $\overline{MS}$  scheme [17]. We note that the uncertainties arising from perturbative matching will be significantly reduced in ratios of nonperturbative matrix elements [17, 43] and that, in general, many HISQ parameters exhibit better perturbative convergence than their AsqTad counterparts [22].

These matching coefficients are critical ingredients in the determination of neutral  $B$  meson mixing on the lat-

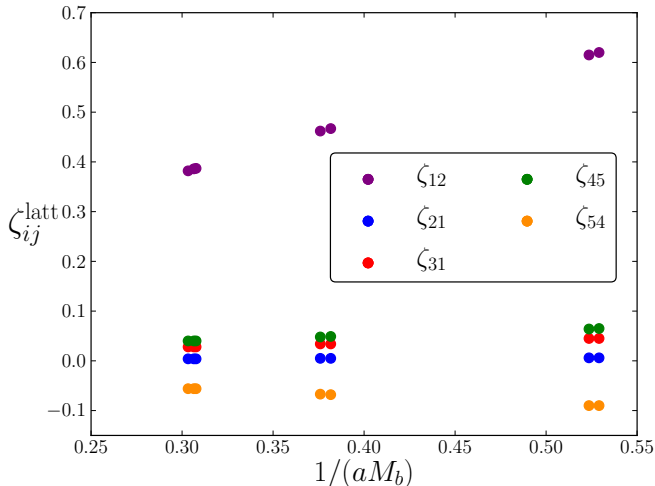


FIG. 10. Mass dependence of the next-to-leading order matching coefficients  $\zeta_{ij}$ , for  $i \neq j$  [color online]. Statistical uncertainties from numerical integration are  $\pm 0.002$  and smaller than the data points on this scale.

tice using NRQCD and HISQ quarks. Without these coefficients, matrix elements calculated nonperturbatively on the lattice cannot be related to experimentally relevant results in continuum QCD in the  $\overline{MS}$  scheme. Since any lattice calculation of neutral meson mixing that incorporates an effective theory description of the heavy quark requires some matching procedure, we have included full details of the lattice perturbation theory calculation, not previously available in the literature, as an aid to future calculations.

Although recent work on the decays of the  $B_s$  meson have been carried out using the relativistic HISQ action for  $b$  and  $s$  quarks [44], such calculations are currently prohibitively expensive for the  $B_d$  meson. Furthermore, computations at the physical  $b$  quark mass are not yet possible and an HQET-guided expansion up to the physical point is still required. Therefore, the use of effective theories for heavy-light systems remains the most practical method for precise predictions of neutral  $B$  meson mixing phenomena.

## ACKNOWLEDGMENTS

The authors are particularly grateful to Christine Davies for useful discussions regarding the one loop continuum calculation. We would also like to thank Georg von Hippel and Peter Lepage for many helpful discussions during the course of this project and Chris Bouchard for reading an early version of the manuscript. This work was supported in part by the U.S. DOE, Grants DE-FG02-04ER41302 and DE-SC0011726. E.G. is supported in part by MINECO (Spain) under Grants FPA2010-16696 and FPA2006-05294; by Junta

de Andalucía (Spain) under Grants FQM-101 and FQM-6552; and by the European Commission under Grant PCIG10-GA-2011-303781. Some of the computing was undertaken on the Darwin supercomputer at the HPCS, University of Cambridge, as part of the DiRAC facility jointly funded by the STFC, and on the sporades cluster at the College of William and Mary.

## Appendix A: Comments on the continuum one loop calculation

In this appendix we give some details of the continuum one loop calculations entering the matching procedure. We focus mainly on scheme dependence, particularly in the “SLL sector”, the sector that covers operators  $Q2$  and  $Q3$ . The continuum results given in Section V A appeared in [19] and expressions for  $c_{11}$ ,  $c_{12}$ ,  $c_{22}$  and  $c_{21}$  were first published in [23]. For those calculations the BBGLN scheme [42] was used in the SLL sector. In an appendix of [19] results were also presented in the SLL sector in the BMU scheme [45], another popular scheme, denoted  $\tilde{c}_{22}$ ,  $\tilde{c}_{21}$ ,  $\tilde{c}_{33}$  and  $\tilde{c}_{31}$ . We have since discovered errors in results for  $\tilde{c}_{33}$  and  $\tilde{c}_{31}$  and correct them here.

We use the NDR- $\overline{MS}$  scheme to regularize ultraviolet divergences. We employ a gluon mass,  $\lambda$ , to handle infrared divergences, as in the lattice calculations. To fix a renormalization scheme completely within Dimensional Regularization of four-fermion operators, one must also specify one’s choices of “evanescent” operators, which enter the calculations as counterterms. Hence one starts from a specific basis of physical operators and then lists the evanescent operators that arise when one tries to project complicated Dirac structures in loop diagrams back onto the physical basis. Most calculations in the literature follow the renormalization procedures with evanescent operators of Buras and Weisz [46]. For one loop calculations it is more convenient to list projections onto the physical basis for the various Dirac structures encountered. Then the evanescent operators are defined as the difference between left-hand and right-hand sides of these projection relations. The evanescent operators vanish in  $d = 4$  dimensions by construction, and for  $d \neq 4$  dimensions they are understood to be subtracted away through the renormalization process. In the Buras and Weisz renormalization scheme [46], equations explicitly involving evanescent operators will become relevant only at two loops. Even at one loop, however, and staying within the framework of the Buras and Weisz renormalization scheme, the set of evanescent operators is not unique. Different projections correspond to different evanescent operators being subtracted by the renormalization procedure. Different projections also lead to different finite contributions to the matching coefficients (the  $c_{ij}$ ’s), although the one loop anomalous dimensions remain the same.

### 1. Examples from the VLL sector

Essentially all continuum calculations used in phenomenology are in agreement on the choices for evanescent operators relevant for  $Q1$ ,  $Q4$  and  $Q5$ . A well known projection relation, for instance, in the  $Q1$  sector (also called the “VLL sector”), is given by,

$$[\gamma_\mu \gamma_\nu \gamma_\rho P_L \otimes \gamma^\mu \gamma^\nu \gamma^\rho P_L] = (16 - 2\epsilon) [\gamma_\rho P_L \otimes \gamma^\rho P_L], \quad (\text{A1})$$

where we use  $d = 4 - \epsilon$  and  $P_L \equiv 1 - \gamma_5$ . Equation (A1) is equivalent to defining and writing down the evanescent operator,

$$E_2^{\text{VLL}} = \left( \bar{\Psi}_b^i \gamma_\mu \gamma_\nu \gamma_\rho P_L \Psi_q^i \right) \left( \bar{\Psi}_b^j \gamma^\mu \gamma^\nu \gamma^\rho P_L \Psi_q^j \right) - (16 - 2\epsilon) Q1. \quad (\text{A2})$$

Another evanescent operator in the VLL sector is

$$E_1^{\text{VLL}} = \left( \bar{\Psi}_b^i \gamma_\rho P_L \Psi_q^j \right) \left( \bar{\Psi}_b^j \gamma^\rho P_L \Psi_q^i \right) - Q1. \quad (\text{A3})$$

In order to write the “projection” version of this definition we work with Dirac structures  $[\Gamma_a \otimes \Gamma_b]$  sandwiched between external spinors. This allows us to take the different color contractions (e.g. “ $ijj$ ” or “ $iji$ ”) into account. In other words if,

$$\left\langle \left( \bar{\Psi}_1^i \Gamma_a \Psi_2^i \right) \left( \bar{\Psi}_3^j \Gamma_b \Psi_4^j \right) \right\rangle_{\text{tree}} = [\bar{u}_1 \Gamma_a u_2] [\bar{u}_3 \Gamma_b u_4], \quad (\text{A4})$$

then

$$\left\langle \left( \bar{\Psi}_1^i \Gamma_a \Psi_2^j \right) \left( \bar{\Psi}_3^j \Gamma_b \Psi_4^i \right) \right\rangle_{\text{tree}} = -[\bar{u}_1 \Gamma_a u_4] [\bar{u}_3 \Gamma_b u_2]. \quad (\text{A5})$$

This step appears between Equations (10) and (11) in the main text. In this notation the projection version of Equation (A3) becomes

$$[\bar{u}_1 \gamma_\rho P_L u_4] [\bar{u}_3 \gamma^\rho P_L u_2] = -[\bar{u}_1 \gamma_\rho P_L u_2] [\bar{u}_3 \gamma^\rho P_L u_4] - \langle E_1^{\text{VLL}} \rangle. \quad (\text{A6})$$

Again the operator  $\langle E_1^{\text{VLL}} \rangle$  is subtracted away in most renormalization schemes and does not contribute in Equation (A6) (see appendices A and B of reference [47] that discuss this point). We have used projections such as (A1) and (A6) in deriving  $c_{11}$  and  $c_{12}$  of Section V A.

### 2. The SLL sector in the BBGLN scheme

We turn next to the SLL sector, which includes operators such as  $Q2$  and  $Q3$  and also, in some schemes, the tensor operator

$$QT \equiv \left( \bar{\Psi}_b^i \sigma_{\mu\nu} P_L \Psi_q^i \right) \left( \bar{\Psi}_b^j \sigma^{\mu\nu} P_L \Psi_q^j \right), \quad (\text{A7})$$

where  $\sigma_{\mu\nu} = \frac{1}{2}[\gamma_\mu, \gamma_\nu]$ . As mentioned earlier, our continuum results for  $c_{22}$ ,  $c_{21}$ ,  $c_{33}$  and  $c_{31}$  in Section V A are

given in the “BBGLN” scheme, introduced in [42]. This scheme uses  $Q2$  and  $Q3$  as the physical operator basis. Equation (15) of [42] defines their evanescent operators in the SLL sector through the following projection:

$$\begin{aligned} [\bar{u}_1 \gamma_\mu \gamma_\nu P_L u_2] [\bar{u}_3 \gamma^\mu \gamma^\nu P_L u_4] = & \\ & 2(4 - \epsilon) [\bar{u}_1 P_L u_2] [\bar{u}_3 P_L u_4] \\ & - 4(2 - \epsilon) [\bar{u}_1 P_L u_4] [\bar{u}_3 P_L u_2]. \end{aligned} \quad (\text{A8})$$

Equivalently one can list the evanescent operators

$$E_1^{\text{SLL}} = \left( \bar{\Psi}_b^i \gamma_\mu \gamma_\nu P_L \Psi_q^i \right) \left( \bar{\Psi}_b^j \gamma^\mu \gamma^\nu P_L \Psi_q^j \right) - 2(4 - \epsilon) Q2 - 4(2 - \epsilon) Q3, \quad (\text{A9})$$

and

$$E_2^{\text{SLL}} = \left( \bar{\Psi}_b^i \gamma_\mu \gamma_\nu P_L \Psi_q^j \right) \left( \bar{\Psi}_b^j \gamma^\mu \gamma^\nu P_L \Psi_q^i \right) - 2(4 - \epsilon) Q3 - 4(2 - \epsilon) Q2. \quad (\text{A10})$$

Using projections such as (A8), we first calculate the one loop corrections to  $Q2$  and  $Q3$ , including the mixing between these two operators. This gives

$$\left( \begin{array}{c} \langle Q2 \rangle \\ \langle Q3 \rangle \end{array} \right)_{\overline{\text{MS}}} = [I + \alpha_s \widehat{M}] \left( \begin{array}{c} \langle Q2 \rangle \\ \langle Q3 \rangle \end{array} \right)_{\text{tree}} \quad (\text{A11})$$

with

$$\widehat{M} = \begin{pmatrix} c'_{22} & c'_{23} \\ c'_{32} & c'_{33} \end{pmatrix}. \quad (\text{A12})$$

We note that these are the full continuum QCD results, with external momenta  $p_q = 0$  for the light quarks and  $p_Q = (\pm M, \vec{0})$  for the heavy (anti-)quarks. The on-shell spinors obeying  $\bar{u}_Q p^\mu \gamma_\mu = M \bar{u}_Q$  and  $\bar{v}_Q p^\mu \gamma_\mu = -M \bar{v}_Q$  then also obey  $\bar{u}_Q \gamma_0 = \bar{u}_Q$  and  $\bar{v}_Q \gamma_0 = -\bar{v}_Q$ . This allows us to use the large  $M$  relation,

$$\langle Q2 \rangle_{\text{tree}} + \langle Q3 \rangle_{\text{tree}} + \frac{1}{2} \langle Q1 \rangle_{\text{tree}} = 0. \quad (\text{A13})$$

So, the  $c_{ij}$  in Section V A for the VLL+SLL sector become

$$c_{22} = c'_{22} - c'_{23}, \quad c_{21} = -\frac{1}{2} c'_{23}, \quad (\text{A14})$$

$$c_{33} = c'_{33} - c'_{32}, \quad c_{31} = -\frac{1}{2} c'_{32}. \quad (\text{A15})$$

### 3. The SLL sector in the BMU scheme

The “BMU” scheme picks  $Q2$  and  $QT$  for the physical basis in the SLL sector. Reference [47] presents a very convenient set of projections for this scheme in their Appendix B, which covers the full basis,  $Q1$ ,  $Q2$ ,  $QT$ ,  $Q4$

and  $Q6$ . Here we reproduce just those for the SLL sector.

$$[\gamma_\mu \gamma_\nu P_L \otimes \gamma^\mu \gamma^\nu P_L] = (4 - \epsilon) [P_L \otimes P_L] + [\sigma_{\mu\nu} P_L \otimes \sigma^{\mu\nu} P_L] \quad (\text{A16})$$

$$[\gamma_\mu \gamma_\nu P_L \otimes \gamma^\nu \gamma^\mu P_L] = (4 - \epsilon) [P_L \otimes P_L] - [\sigma_{\mu\nu} P_L \otimes \sigma^{\mu\nu} P_L] \quad (\text{A17})$$

$$[\sigma_{\mu\nu} \gamma_\alpha \gamma_\beta P_L \otimes \sigma^{\mu\nu} \gamma^\alpha \gamma^\beta P_L] = (48 - 40\epsilon) [P_L \otimes P_L] + (12 - 3\epsilon) [\sigma_{\mu\nu} P_L \otimes \sigma^{\mu\nu} P_L] \quad (\text{A18})$$

$$[\sigma_{\mu\nu} \gamma_\alpha \gamma_\beta P_L \otimes \gamma^\beta \gamma^\alpha \sigma^{\mu\nu} P_L] = -(48 - 40\epsilon) [P_L \otimes P_L] + (12 - 7\epsilon) [\sigma_{\mu\nu} P_L \otimes \sigma^{\mu\nu} P_L] \quad (\text{A19})$$

Note that since all five operators in this basis have the same color structure, we do not need to include external spinors in the projection relations. Instead of Equation (A11), we now have

$$\left( \begin{array}{c} \langle Q2 \rangle \\ \langle QT \rangle \end{array} \right)_{\overline{\text{MS}}} = [I + \alpha_s \widehat{M}_{2T}] \left( \begin{array}{c} \langle Q2 \rangle \\ \langle QT \rangle \end{array} \right)_{\text{tree}}, \quad (\text{A20})$$

with

$$\widehat{M}_{2T} = \begin{pmatrix} \tilde{c}'_{22} & \tilde{c}'_{2T} \\ \tilde{c}'_{T2} & \tilde{c}'_{TT} \end{pmatrix}. \quad (\text{A21})$$

One can now rotate to the  $Q2$ ,  $Q3$  basis so that

$$\left( \begin{array}{c} \langle Q2 \rangle \\ \langle Q3 \rangle \end{array} \right)_{\text{tree}} = \widehat{R} \left( \begin{array}{c} \langle Q2 \rangle \\ \langle QT \rangle \end{array} \right)_{\text{tree}}, \quad \widehat{M}_{Q23} = \widehat{R} \widehat{M}_{2T} \widehat{R}^{-1}, \quad (\text{A22})$$

where

$$\widehat{R} = \begin{pmatrix} 1 & 0 \\ -\frac{1}{2} & \frac{1}{8} \end{pmatrix}. \quad (\text{A23})$$

Finally we use Equation (A13) once again to obtain  $\tilde{c}_{22}$ ,  $\tilde{c}_{21}$ ,  $\tilde{c}_{33}$ ,  $\tilde{c}_{31}$  in the BMU scheme. The updated and corrected results are:

$$\tilde{c}_{22} = \frac{1}{4\pi} \left\{ 6 + \frac{16}{3} \log \frac{\mu^2}{M^2} - \frac{4}{3} \log \frac{\lambda^2}{M^2} \right\} \quad (\text{A24})$$

$$\tilde{c}_{21} = \frac{1}{4\pi} \left\{ \frac{4}{3} + \frac{1}{3} \log \frac{\mu^2}{M^2} + \frac{2}{3} \log \frac{\lambda^2}{M^2} \right\} \quad (\text{A25})$$

$$\tilde{c}_{33} = \frac{1}{4\pi} \left\{ -\frac{2}{3} - \frac{8}{3} \log \frac{\mu^2}{M^2} - \frac{4}{3} \log \frac{\lambda^2}{M^2} \right\} \quad (\text{A26})$$

$$\tilde{c}_{31} = \frac{1}{4\pi} \left\{ \frac{17}{6} + \frac{4}{3} \log \frac{\mu^2}{M^2} + \frac{2}{3} \log \frac{\lambda^2}{M^2} \right\}. \quad (\text{A27})$$

As expected, the anomalous dimension terms and infrared logarithms are the same as in the BBGLN scheme.

- 
- [1] T. Aaltonen *et al.* (CDF Collaboration), Phys.Rev.Lett. **109**, 171802 (2012), arXiv:1208.2967 [hep-ex].
- [2] T. Aaltonen *et al.* (CDF Collaboration), Phys.Rev. **D85**, 072002 (2012), arXiv:1112.1726 [hep-ex].
- [3] V. M. Abazov *et al.* (D0 Collaboration), Phys.Rev. **D89**, 012002 (2014), arXiv:1310.0447 [hep-ex].
- [4] V. M. Abazov *et al.* (D0 Collaboration), Phys.Rev. **D86**, 072009 (2012), arXiv:1208.5813 [hep-ex].
- [5] V. M. Abazov *et al.* (D0 Collaboration), Phys.Rev.Lett. **105**, 081801 (2010), arXiv:1007.0395 [hep-ex].
- [6] R. Aaij *et al.* (LHCb collaboration), Eur.Phys.J. **C73**, 2655 (2013), arXiv:1308.1302 [hep-ex].
- [7] R. Aaij *et al.* (LHCb Collaboration), Phys.Lett. **B719**, 318 (2013), arXiv:1210.6750 [hep-ex].
- [8] E. Lunghi and A. Soni, Phys.Lett. **B697**, 323 (2011), arXiv:1010.6069 [hep-ph].
- [9] A. Lenz, U. Nierste, J. Charles, S. Descotes-Genon, H. Lacker, *et al.*, Phys.Rev. **D86**, 033008 (2012), arXiv:1203.0238 [hep-ph].
- [10] J. Laiho, E. Lunghi, and R. Van De Water, PoS **FPCP2010**, 040 (2010), arXiv:1102.3917 [hep-ph].
- [11] A. Lenz, U. Nierste, J. Charles, S. Descotes-Genon, A. Jantsch, *et al.*, Phys.Rev. **D83**, 036004 (2011), arXiv:1008.1593 [hep-ph].
- [12] E. Lunghi and A. Soni, Phys.Rev.Lett. **104**, 251802 (2010), arXiv:0912.0002 [hep-ph].
- [13] Y. Aoki, T. Ishikawa, T. Izubuchi, C. Lehner, and A. Soni, (2014), arXiv:1406.6192 [hep-lat].
- [14] C. Chang, C. Bernard, C. Bouchard, A. El-Khadra, E. Freeland, *et al.*, (2013), arXiv:1311.6820 [hep-lat].
- [15] T. Ishikawa, Y. Aoki, T. Izubuchi, C. Lehner, and A. Soni, (2013), arXiv:1312.1010 [hep-lat].
- [16] A. Bazavov, C. Bernard, C. Bouchard, C. DeTar, M. Di Pierro, *et al.*, Phys.Rev. **D86**, 034503 (2012), arXiv:1205.7013 [hep-lat].
- [17] E. Gamiz, C. T. H. Davies, G. P. Lepage, J. Shigemitsu, M. Wingate (HPQCD Collaboration), Phys.Rev. **D80**, 014503 (2009), arXiv:0902.1815 [hep-lat].
- [18] HPQCD Collaboration, *in preparation*.
- [19] E. Gamiz, J. Shigemitsu, and H. Trottier, Phys.Rev. **D77**, 114505 (2008), arXiv:0804.1557 [hep-lat].
- [20] R. Dowdall *et al.* (HPQCD Collaboration), Phys.Rev. **D85**, 054509 (2012), arXiv:1110.6887 [hep-lat].
- [21] T. C. H. Hammant, A. Hart, G. von Hippel, R. Horgan, and C. Monahan, Phys.Rev. **D88**, 014505 (2013), arXiv:1303.3234 [hep-lat].
- [22] C. Monahan, J. Shigemitsu, and R. Horgan, Phys.Rev. **D87**, 034017 (2013), arXiv:1211.6966 [hep-lat].
- [23] S. Hashimoto, K. Ishikawa, T. Onogi, M. Sakamoto, N. Tsutsui, *et al.*, Phys.Rev. **D62**, 114502 (2000), arXiv:hep-lat/0004022 [hep-lat].

- [24] K. Ishikawa, T. I. Onogi, and N. Yamada, *Phys.Rev.* **D60**, 034501 (1999), arXiv:hep-lat/9812007 [hep-lat].
- [25] O. Laktik and T. Izubuchi, *Phys.Rev.* **D75**, 034504 (2007), arXiv:hep-lat/0612022 [hep-lat].
- [26] N. H. Christ, T. T. Dumitrescu, O. Laktik, and T. Izubuchi, *PoS LATT2007*, 351 (2007), arXiv:0710.5283 [hep-lat].
- [27] T. Ishikawa, Y. Aoki, J. M. Flynn, T. Izubuchi, and O. Laktik, *JHEP* **1105**, 040 (2011), arXiv:1101.1072 [hep-lat].
- [28] M. Papinutto, G. Herdoiza, C. Pena, and A. Vladikas, *PoS LATTICE2013*, 317 (2013), arXiv:1311.5177 [hep-lat].
- [29] F. Gabbiani, E. Gabrielli, A. Masiero, and L. Silvestrini, *Nucl.Phys.* **B477**, 321 (1996), arXiv:hep-ph/9604387 [hep-ph].
- [30] C. Itzykson and J. Zuber, *Quantum Field Theory* (Dover, 1980).
- [31] S. Collins, C. Davies, J. Hein, G. Lepage, C. Morningstar, *et al.*, *Phys.Rev.* **D63**, 034505 (2001), arXiv:hep-lat/0007016 [hep-lat].
- [32] C. J. Morningstar and J. Shigemitsu, *Phys.Rev.* **D57**, 6741 (1998), arXiv:hep-lat/9712016 [hep-lat].
- [33] P. Weisz, *Nucl.Phys.* **B212**, 1 (1983).
- [34] P. Weisz and R. Wohlert, *Nucl.Phys.* **B236**, 397 (1984).
- [35] G. Curci, P. Menotti, and G. Paffuti, *Phys.Lett.* **B130**, 205 (1983).
- [36] Lüscher, M. and P. Weisz, *Phys.Lett.* **B158**, 250 (1985).
- [37] E. Follana *et al.* (HPQCD Collaboration, UKQCD Collaboration), *Phys.Rev.* **D75**, 054502 (2007), arXiv:hep-lat/0610092 [hep-lat].
- [38] A. Hart, G. von Hippel, R. Horgan, and L. Storoni, *J.Comput.Phys.* **209**, 340 (2005), arXiv:hep-lat/0411026 [hep-lat].
- [39] A. Hart, G. von Hippel, R. Horgan, and E. Muller, *Comput.Phys.Commun.* **180**, 2698 (2009), arXiv:0904.0375 [hep-lat].
- [40] E. Gulez, J. Shigemitsu, and M. Wingate, *Phys.Rev.* **D69**, 074501 (2004), arXiv:hep-lat/0312017 [hep-lat].
- [41] C.J. Morningstar, *Phys. Rev. D* **48**, 2265 (1993).
- [42] M. Beneke, G. Buchalla, C. Greub, A. Lenz, and U. Nierste, *Phys.Lett.* **B459**, 631 (1999), arXiv:hep-ph/9808385 [hep-ph].
- [43] H. Na, C. J. Monahan, C. T. Davies, R. Horgan, G. P. Lepage, and J. Shigemitsu, *Phys.Rev.* **D86**, 034506 (2012), arXiv:1202.4914 [hep-lat].
- [44] C. McNeile, C. T. H. Davies, E. Follana, K. Hornbostel, and G. P. Lepage, *Phys.Rev.* **D85**, 031503 (2012), arXiv:1110.4510 [hep-lat].
- [45] A. J. Buras, M. Misiak, and J. Urban, *Nucl.Phys.* **B586**, 397 (2000), arXiv:hep-ph/0005183 [hep-ph].
- [46] A. J. Buras and P. H. Weisz, *Nucl.Phys.* **B333**, 66 (1990).
- [47] A. J. Buras and J. Girkbach, *JHEP* **1203**, 052 (2012), arXiv:1201.1302 [hep-ph].